

Electronic Supplementary Information

Versatile, Transferrable 3-Dimensionally-Nanofabricated Au Catalysts with High-Index Crystal Planes for Highly Efficient and Robust Electrochemical CO₂ Reduction

Minhyung Cho^{§a}, Jong Min Kim^{§a}, Beomil Kim^a, Soonmin Yim^a, Ye Ji Kim^a, Yeon Sik Jung^{*a}, and Jihun Oh^{*abc}

^a Department of Materials Science and Engineering, Korea Advanced Institute of Science and Technology (KAIST), Daejeon 34141, Republic of Korea

^b Graduate School of Energy, Environment, Water, and Sustainability (EEWS), Korea Advanced Institute of Science and Technology (KAIST), Daejeon 34141, Republic of Korea

^c KAIST Institute for NanoCentury, Korea Advanced Institute of Science and Technology (KAIST), Daejeon 34141, Republic of Korea

E-mail: ysjung@kaist.ac.kr

E-mail: jihun.oh@kaist.ac.kr

§ These authors contributed equally

Experimentation

Master mold preparation

A master mold with 200 nm width and 1.2 μm pitch was fabricated using KrF photolithography followed by reactive ion etching process. To reduce the surface energy before using it as a master mold, hydroxyl-terminated PDMS homopolymer solution (1.5 wt%) purchased from Polymer Source Inc. (Canada) was spin-coated on the master mold and thermal annealed at 200 °C for 2 hours. After thermal annealing, the unattached polymer was washed with heptane.

Solvent-assisted nanotransfer printing process and sample preparation

PMMA homopolymer purchased from Sigma-Aldrich Inc. was dissolved in a mixed solvent of toluene, acetone, and heptane (4.5:4.5:1 by volume, 4 wt%). A PMMA solution was spin-coated onto the master mold, and PI adhesive film purchased from 3M Inc. was then smoothly attached on the surface of the PMMA replica and detached from the mold. Through oblique-angle deposition (deposition angle = 85°) using an e-beam evaporator, Au NWs were formed on the PMMA replica/PI adhesive film. The Au NWs on the PMMA replica/PI adhesive film were exposed to a mixed solvent vapor (acetone/heptane 1:1 by volume) at 55 °C for 20~30 s and then directly contacted on the receiver substrates and transferred. After the transfer process, the PMMA replica was removed by toluene solvent. The bare Au thin film was prepared by e-beam deposition with normal incidence angle on Si substrates. All prepared multi-stacked Au NWs and bare Au electrodes were sealed with Nitto tape to confine the reactive area and connected with copper wires to apply external bias through a potentiostat. A carbon paper with a microporous layer (SIGRACET, 39BC) was used as a GDE. For the transferring of MS-Au NWs onto a GDE, firstly, MS-Au NWs were prepared on a Cu foil substrate, which was a sacrificial substrate. PMMA polymer as a

transfer medium was spin-coated on the prepared multi-stacked Au NWs on the Cu foil substrate. The top surface of the GDE was treated by O₂ plasma using ICP-RIE to lower the hydrophobicity of the surface. Similar to the well-known graphene transfer process [1], PMMA coated multi-stacked Au NWs were successfully transferred onto the surface-treated GDE using a Cu etchant solution. After transfer to the GDE, the PMMA polymer was removed by washing with toluene solvent.

Characterization

SEM, EBSD, TEM, XPS, XRD

The surface morphologies of all prepared electrodes were investigated by field emission scanning electron microscopy (FE-SEM: Hitachi S-4800, JEOL 7600F) operated at 15 kV. The exposed crystalline facet was observed through electron backscatter diffraction (EBSD) with a Hikari detector in the SEM (Quanta 3D FEG) with 20 kV accelerating voltage. Top-view transmission electron microscopy (TEM) samples were prepared by mechanical polishing, and investigated by TEM (JEOL JEM-ARM200F microscope) operated at 200 kV. Surface chemical composition was analyzed by X-ray photoelectron spectrometer (K-alpha, Thermo VG Scientific), and grain size and crystal information were obtained with a multi-purpose thin-film X-ray diffractometer (RIGAKU).

ECSA Measurement

The electrochemical surface area of all prepared Au electrodes was characterized by surface Au oxidation/reduction reaction [2]. Through cyclic voltammogram (CV), an AuO monolayer was formed on the Au surface toward the anodic potential region and reduced at the cathodic potential region,

sequentially. By integrating reduction charge of the AuO monolayer at around 0.9 V vs. Ag/AgCl, the electroactive surface area of the Au for CO₂RR could be calculated (448 μC cm⁻²). The CV curve scanning was conducted in 0.05 M H₂SO₄ aqueous solution with the range of 0 to 1.5 V vs. Ag/AgCl (50 mV s⁻¹).

CO₂ Reduction Product Analysis

Electrochemical CO₂ reduction experiments were conducted under room temperature and ambient pressure condition with a gas-tight single batch reactor or a flow reactor. For a gas-tight single batch reactor having 40 mL head space volume and 20 mL electrolyte, we used Ag/AgCl in 3M NaCl, graphite rods, and prepared the Au electrodes as a reference electrode, counter electrode, and working electrodes, respectively. For the electrolyte, CO₂-saturated 0.2 M KHCO₃ solution with pH 6.8 was used. The electrolyte in the reactor was stirred at 600 rpm during the reaction. Note that the re-oxidation of evolved CO gas product at the working electrodes in the single batch reactor can be ignored due to poor solubility of CO in water (~ 0.1 mM) [3]. For a flow reactor, 1M KOH solution with pH 13.65 was used as an electrolyte. CO₂ was continuously fed to the backside of a cathode region with 20 sccm, and its gaseous product was captured with a Tedlar gas sampling bag. For reference and counter electrodes, Ag/AgCl in 3M NaCl and Pt foil were used. All the potential written in this paper at single batch reactor results was specified with reversible hydrogen electrode (RHE) scale: $E_{\text{RHE}} = E_{\text{Ag/AgCl}(3\text{M NaCl})} + 0.209 + 0.0591 \times \text{pH}$. All the potential for the flow reactor was specified with reversible hydrogen electrode (RHE) scale: $E_{\text{RHE}} = E_{\text{Ag/AgCl}(\text{sat'd KCl})} + 0.197 + 0.0591 \times \text{pH}$. All captured gaseous products in the head space (gas-tight single batch reactor) or Tedlar bag (flow reactor) of the reactor were characterized by gas chromatography (Inficon, micro GC 3000). High performance liquid chromatography (HPLC, YL instruments, YL9100 HPLC with SUGAR SH1011 column) was used to detect liquid products after CO₂ electrolysis.

Product selectivity

In order to compare CO₂RR activity of the Au electrocatalysts, we use the selectivity which is defined as

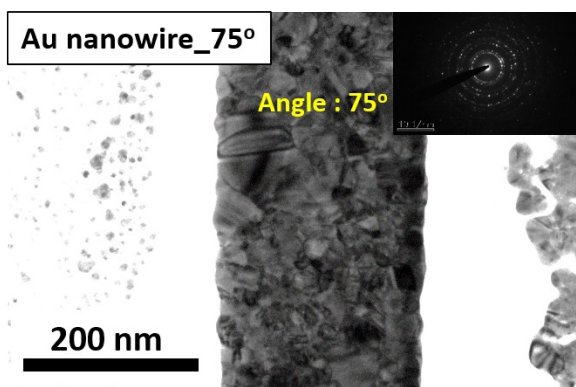
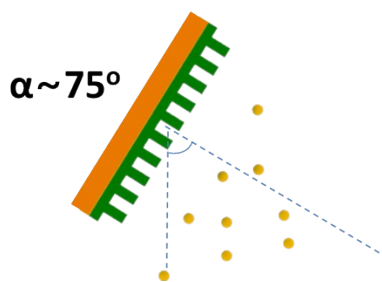
$$\text{selectivity (\%)} = \frac{\text{Product Faraday efficiency (\%)}}{\text{Total Faraday efficiency (\%)}} \times 100. \quad (\text{S1})$$

Since no liquid products were detected after CO₂ electrolysis from HPLC, total F.E. in (S1) includes F.E. of evolved CO and H₂.

Mass activity calculation

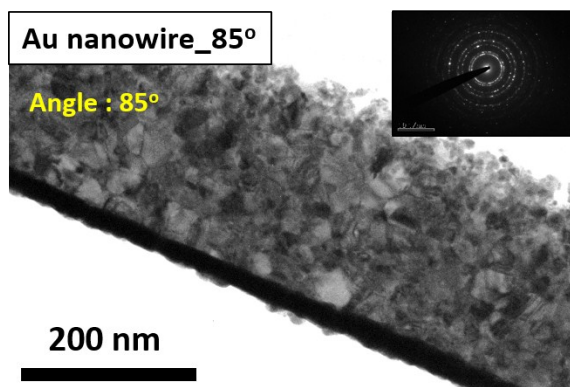
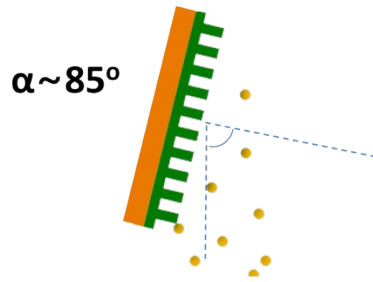
In order to calculate mass activity, we first dissolved 10 layers of MS-Au printed on an 1 cm² glass substrate in a mixture solution of nitric acid and hydrochloric acid and the amount of the dissolved Au in the solution was measured using inductively coupled plasma mass spectrometry (ICP-MS, Agilent, 7700S ICP-MS). The mass activity of MS-Au at -0.19 V were then calculated from the CO₂RR current density at -0.19 V divided by the measured Au mass, which is 4.17 μg/cm²/Au-layer.

a) Deposition angle (75°)



2-Theta (crystalline plane)	Intensity ratio normalized by intensity of (111)
38.172 (111)	1
44.353 (200)	0.076
64.564 (220)	0.057
77.517 (311)	0.056
81.691 (222)	0.041

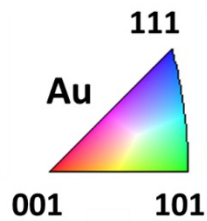
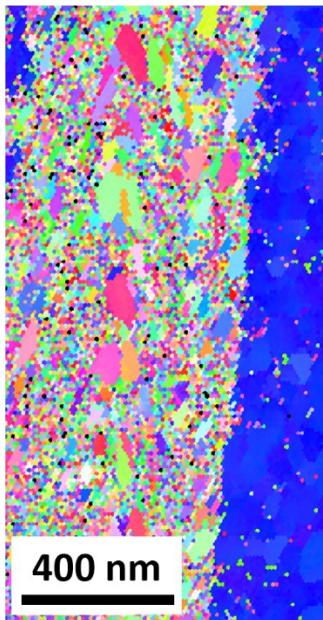
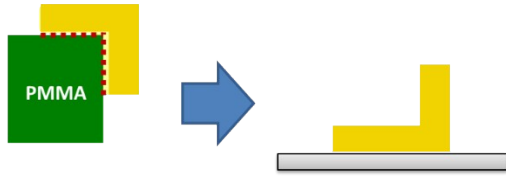
b) Deposition angle (85°)



2-Theta (crystalline plane)	Intensity ratio normalized by intensity of (111)
38.172 (111)	1
44.353 (200)	0.117
64.564 (220)	0.078
77.517 (311)	0.077
81.691 (222)	0.043

Figure S1. TEM images and XRD results of Au NWs depending on deposition angles, a) 75° and b) 85°, respectively. The green color indicates preferential crystal orientation, and the blue color indicates un-preferential crystal orientation.

a) Top surface
(normally transferred)



b) Bottom surface
(inversely transferred)

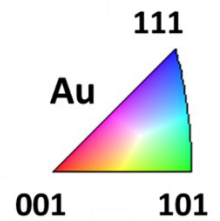
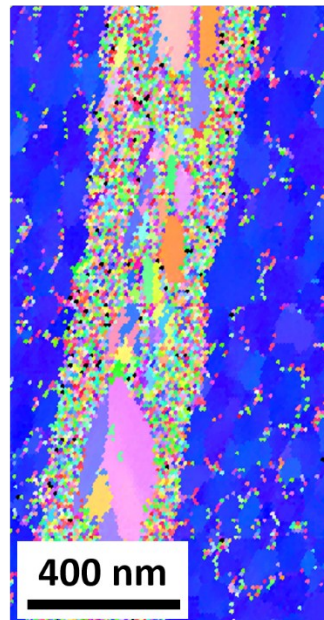
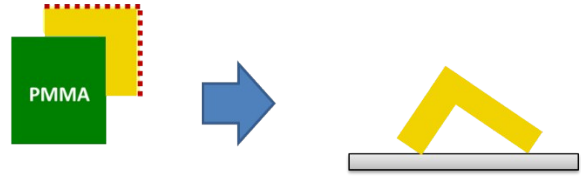


Figure S2. Electron backscattering diffraction (EBSD) results for Au NWs. Color-mapping of a) normally transferred Au NWs and b) inversely transferred Au NWs. For more accurate measurement, Au NWs used in our experiments were fabricated by oblique-angle deposition with 75° .

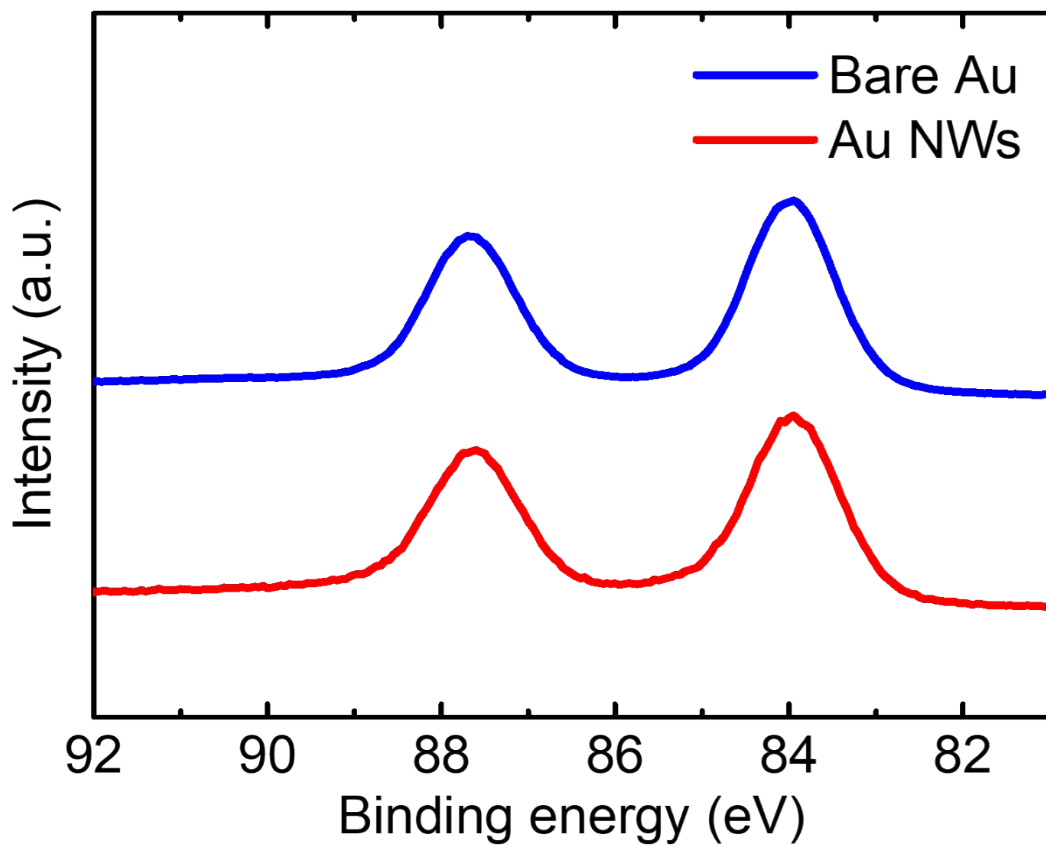


Figure S3. Au 4f X-ray photoelectron spectrometer (XPS) spectra of bare Au and Au nanowires, respectively.

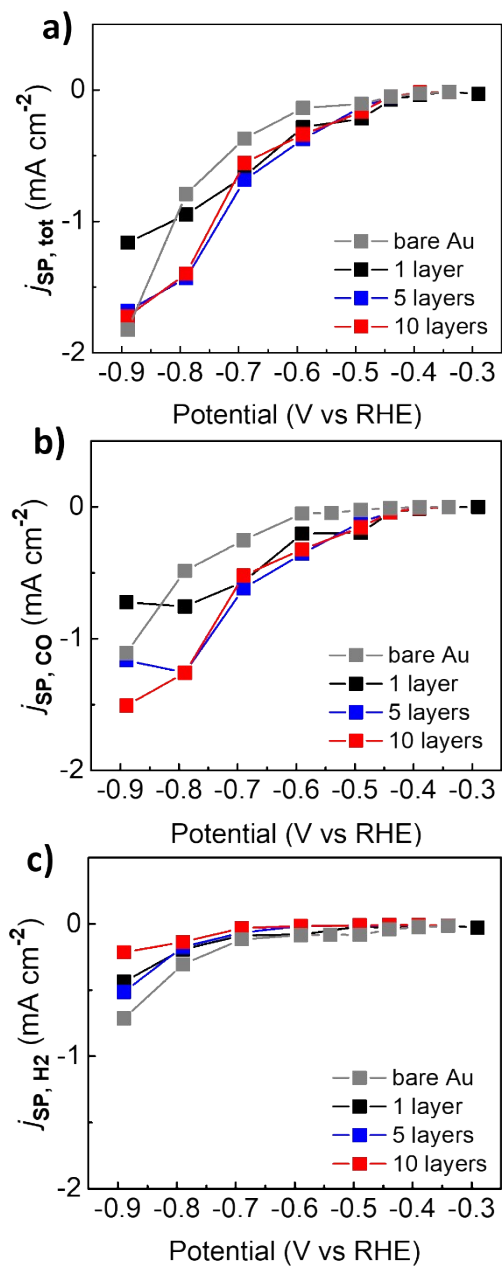


Figure S4. a) Total current density (j_{tot}), b) CO evolving partial current density (j_{CO}), and c) H₂ evolving partial current density (j_{H_2}) of bare Au and MS-Au electrodes. All current densities are denoted as surface-area specific current density.

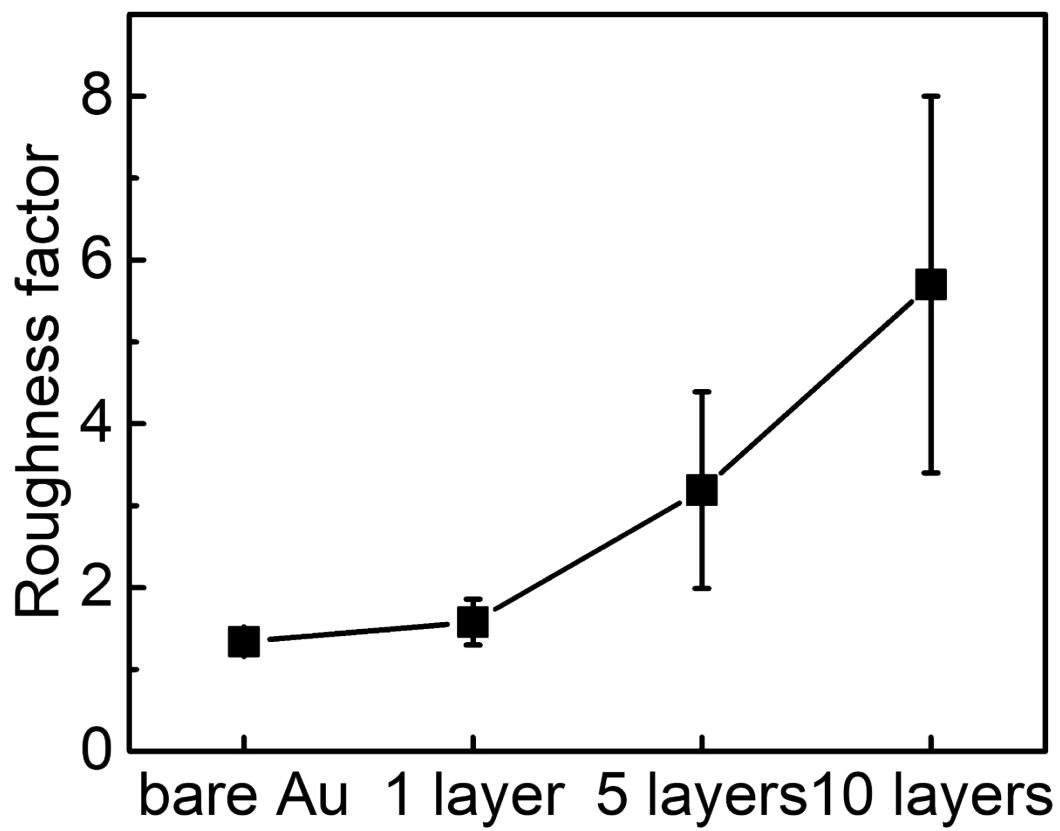


Figure S5. Roughness factor of each electrode (bare Au and MS-Au electrodes).

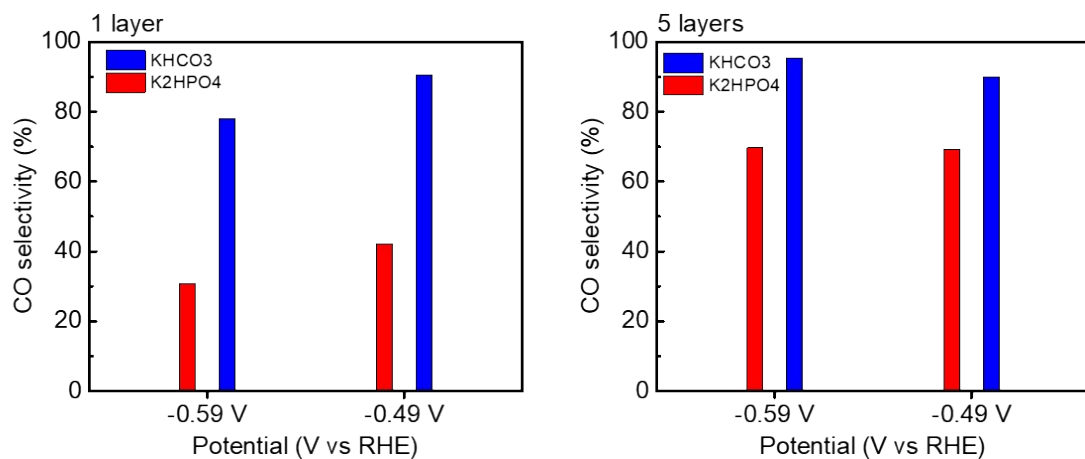


Figure S6. Comparison of the CO selectivity of the 1-layer and 5-layers MS-Au at -0.49 and -0.59 V in CO_2 -saturated 0.2 M K_2HPO_4 (pH ~ 6.8) and 0.2 M KHCO_3 (pH ~ 6.8).

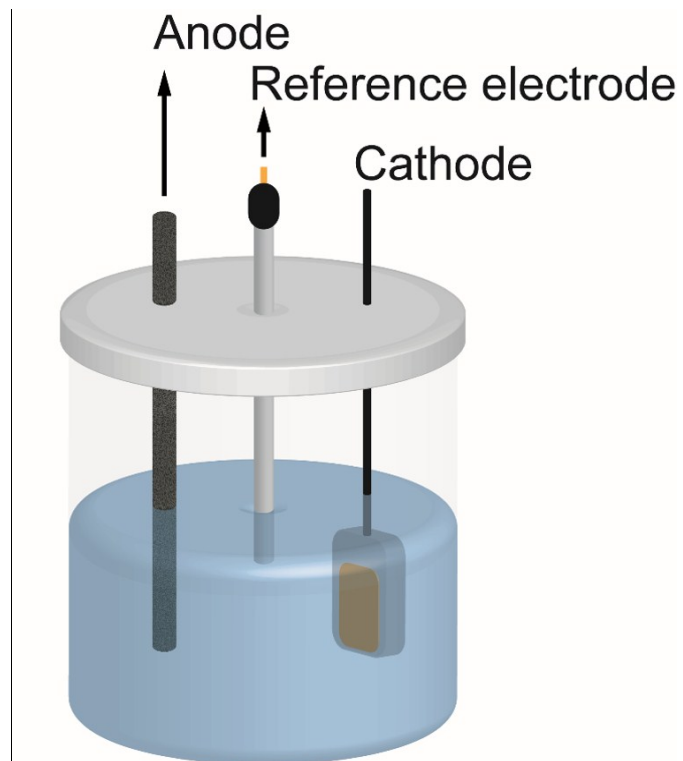


Figure S7. Schematic drawing of gas-tight single batch reactor.

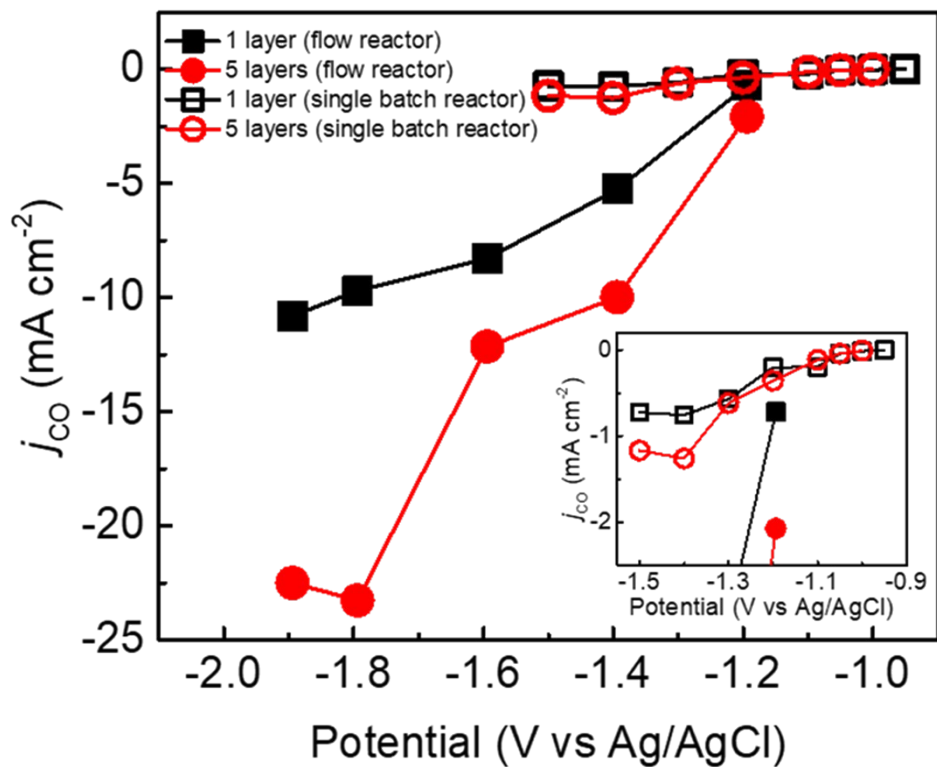


Figure S8. CO evolution current density of 1 and 5 layers of MS-Au in the flow reactor and single batch reactor, expressed in pH-independent Ag/AgCl reference scale. The inset shows j_{CO} near the onset potential.

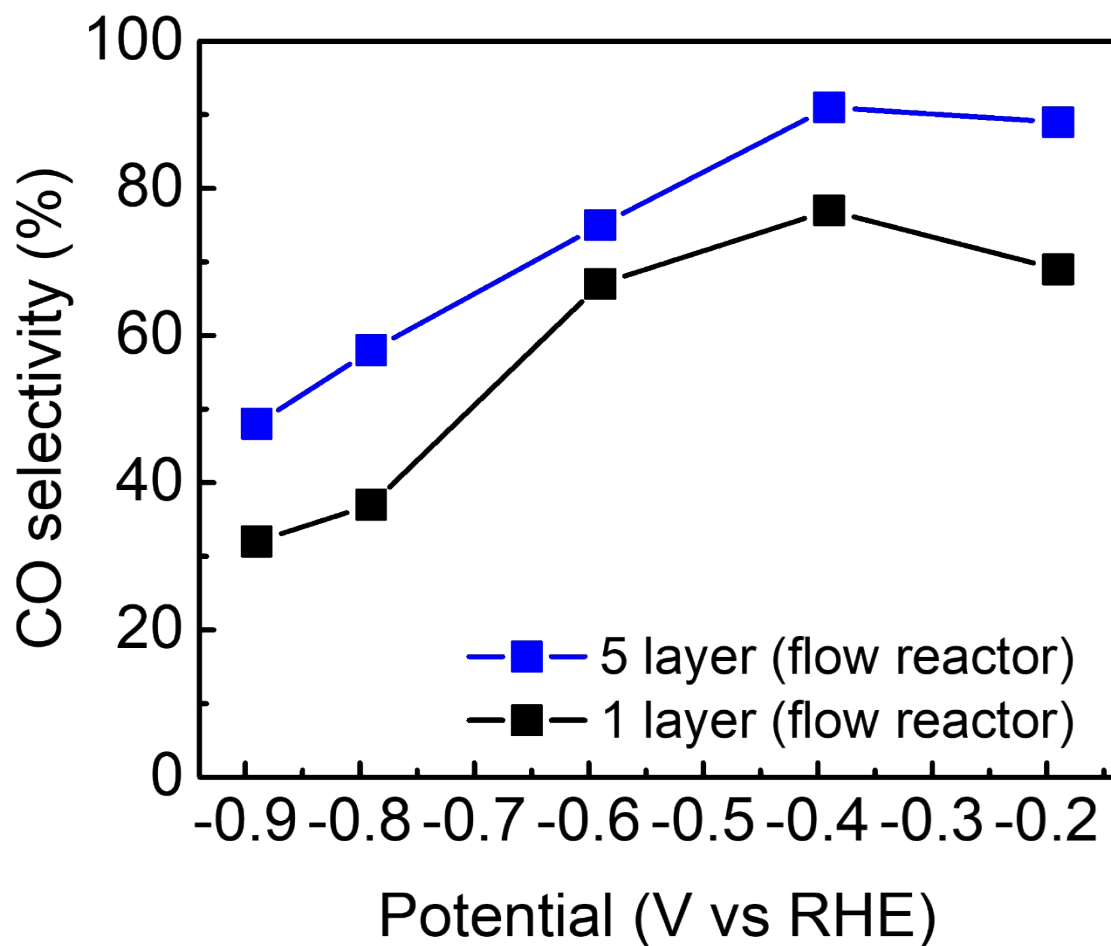


Figure S9. CO selectivity of 1, 5 layers of MS-Au as a function of the applied potential with GDE in flow reactor (electrolyte: 1 M KOH).

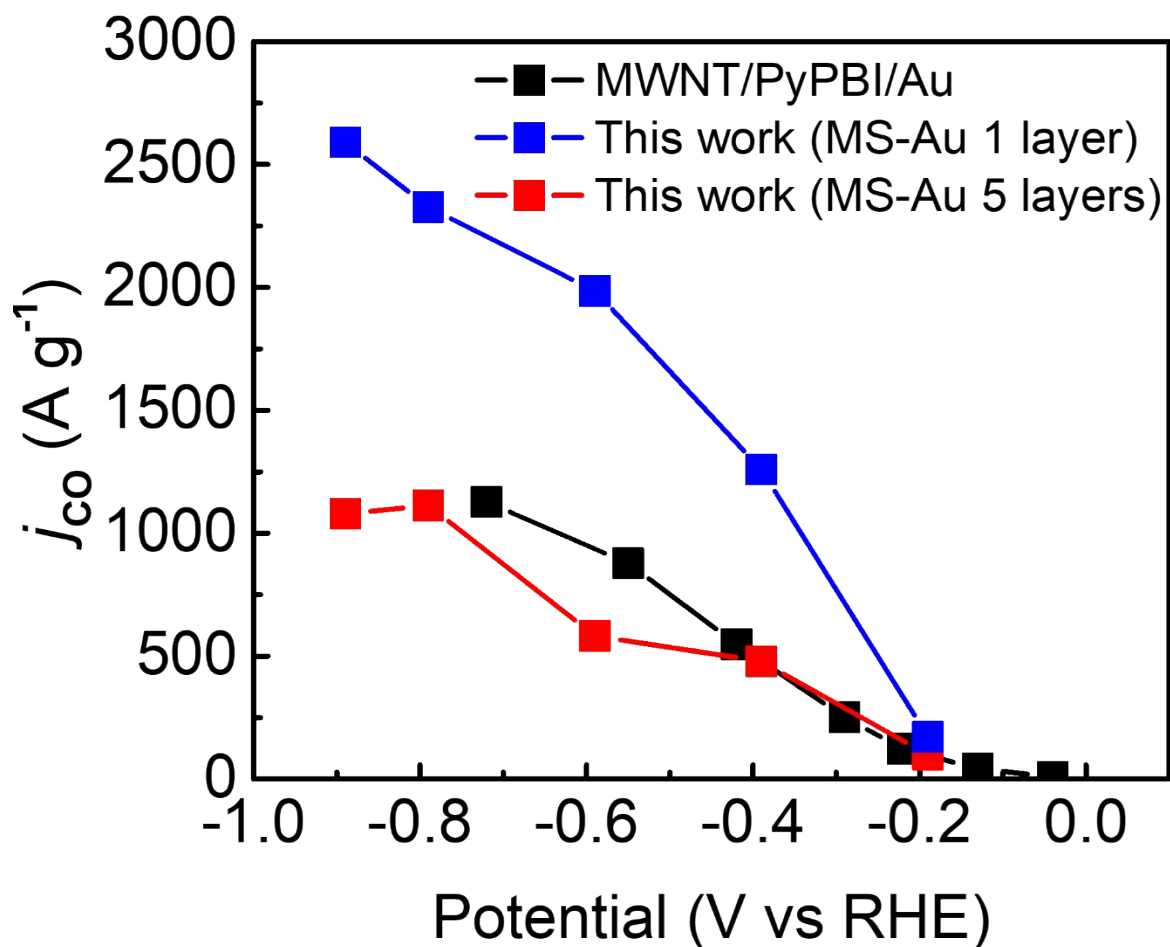


Figure S10. Comparison of mass activity for CO evolution denoted as partial current density j_{CO} ($A\ g^{-1}$) between MS-Au (this work) and poly(2,2'-(2,6-pyridine)-5,5'-bibenzimidazole) polymer wrapped multiwall carbon nanotube (MWNT/PyPBI/Au) [4].

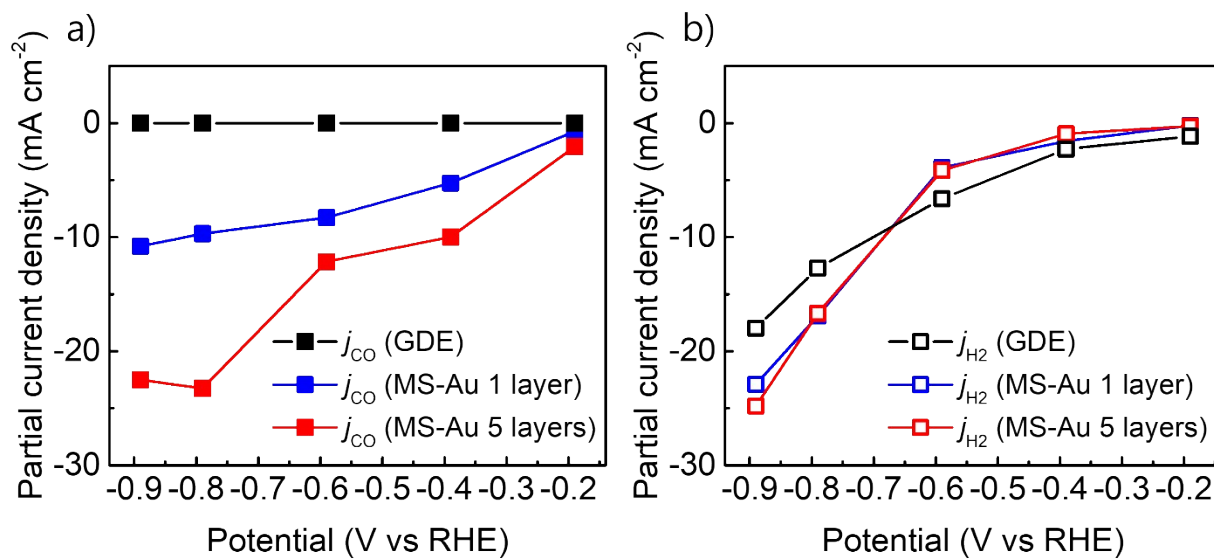


Figure S11. Geometric partial current density of CO evolution (j_{CO}) and H₂ evolution (j_{H_2}) of 1, 5 layers of MS-Au with GDE and bare GDE by itself.

Reference

- [1] Y. Chen, X. L. Gong, J. G. Gai, *Advanced science* **2016**, 3, 1500343.
- [2] M. Liu, Y. Pang, B. Zhang, P. De Luna, O. Voznyy, J. Xu, X. Zheng, C. T. Dinh, F. Fan, C. Cao, F. P. de Arquer, T. S. Safaei, A. Mepham, A. Klinkova, E. Kumacheva, T. Filleter, D. Sinton, S. O. Kelley, E. H. Sargent, *Nature* **2016**, 537, 382.
- [3] G.W.C. Kaye et al, "Tables of Physical and Chemical Constants," 15th ed., Longman, NY, **1986**, p. 219.
- [4] S. Verma, Y. Hamasaki, C. Kim, W. Huang, S. Lu, H.-R. M. Jhong, A. A. Gewirth, T. Fujigaya, N. Nakashima, P. J. Kenis, *ACS Energy Letters* **2018**, 3, 193.